Lipase-Powered Mesoporous Silica Nanomotors for Triglyceride Degradation

Lei Wang+, Ana C. Hortelao+, Xin Huang, and Samuel Sánchez*

March 2019

[*] Dr. L. Wang,[+] Prof. Dr. X. Huang
MIIT Key Laboratory of Critical Materials Technology for New Energy Conversion and Storage
School of Chemistry and Chemical Engineering
Harbin Institute of Technology, Harbin 150001 (China)

Dr. L. Wang,[+] A. C. Hortelao,[+] Prof. Dr. S. Sánchez
Institute for Bioengineering of Catalonia (IBEC)
The Barcelona Institute of Science and Technology (BIST)
Baldiri i Reixac 10–12, 08028 Barcelona (Spain)
E-mail: ssanchez@ibecbarcelona.eu

Prof. Dr. S. Sánchez
Institució Catalana de Recerca i Estudis AvanÅats (ICREA)
Pg. Lluís Companys 23, 08010 Barcelona (Spain)

[+] These authors contributed equally to this work.

Keywords: enzyme nanomotors · lipase · micromotors ·oil removal · self-propulsion

Abstract

Lipase-based nanomotors that are capable of enhanced Brownian motion over long periods of time in triglyceride solution and of degrading triglyceride droplets have been synthesized. The biocatalytic reaction between lipase and its water-soluble oil substrate triacetin as fuel led to about 40 min of enhanced diffusion of lipase-modified mesoporous silica nanoparticles.

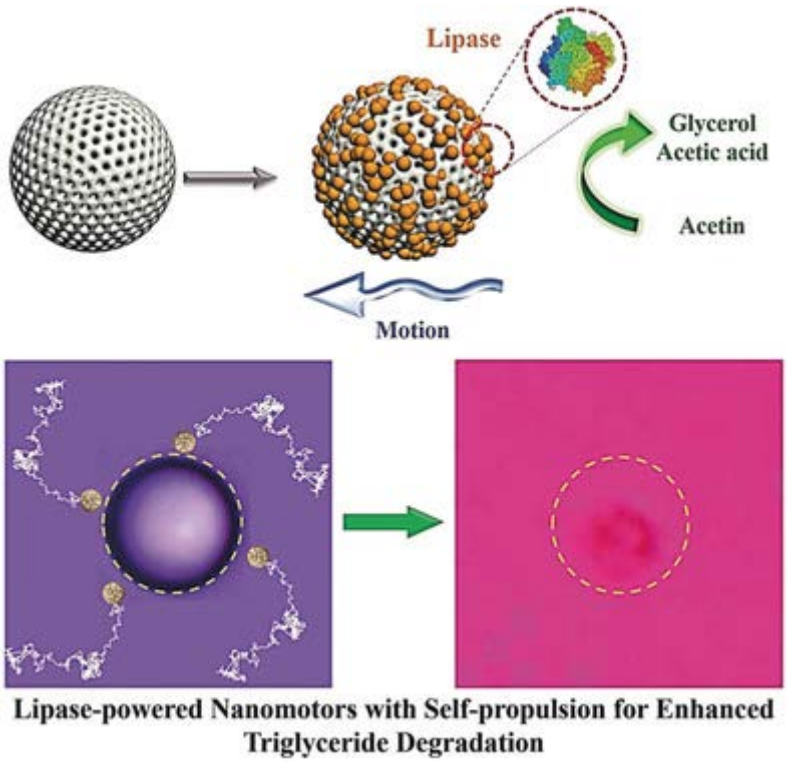

Lipase-powered Nanomotors with Self-propulsion for Enhanced Triglyceride Degradation

We report lipase-based nanomotors that are capable of enhanced Brownian motion over long periods of time in triglyceride solution and of degrading triglyceride droplets that mimic "blood lipids". We achieved about 40 min of enhanced diffusion of lipase-modified mesoporous silica nanoparticles (MSNPs) through a biocatalytic reaction between lipase and its corresponding water-soluble oil substrate (triacetin) as fuel, which resulted in an enhanced diffusion coefficient (ca. 50 % increase) at low triacetin concentration (<10 mm). Lipase not only serves as the power engine but also as a highly efficient cleaner for the triglyceride droplets (e.g., tributyrin) in PBS solution, which could yield potential biomedical applications, for example, for dealing with diseases related to the accumulation of triglycerides, or for environmental remediation, for example, for the degradation of oil spills.

Synthetic micro/nanomotors are active colloids that self-propel in fluids while performing complex tasks such as cargo pick-up and release,[1] sensing,[2] biomedical applications,[3] and environmental remediation.[4] There are several methods to trigger the propulsion of micro/nanomotors, including through catalytic reactions,[5] electric fields,[6] as well as ultrasonic,[7] magnetic,[8] and light excitation.[9] Particularly for in vivo applications, it is necessary to explore biocompatible and biomimetic designs that are capable of actuating in biological systems without side effects. Therefore, enzymes that carry out energy conversion in biological systems by using existing fuel sources, and without requiring an external power source, are good candidates to address these concerns.[10] Sen and co-workers provided experimental evidence of enhanced single-enzyme diffusion based on substrate turnover.[11] They also demonstrated molecular chemotaxis of urease and catalase towards a gradient of increasing substrate concentrations,[11b] as well as the fabrication of enzymatic motors.[12] Our group extended this field by modifying Janus mesoporous silica micro/nanoparticles with different enzymes.[13] With urease, the hollow Janus silica micromotors achieved a directional propulsion with a high degree of controllability, either through the addition of salts or in the presence of a magnetic field.[13b] In addition, we reported how the stochastic binding of enzymes to the surface of the

particles with a molecular asymmetry in enzyme distribution results in an asymmetric generation of forces, which in turn leads to self-propulsion.[14] This technique was also adopted for the fabrication of nanomotors based on mesoporous silica nanoparticles, which yielded a more efficient delivery and release system of anticancer drugs to cells in vitro, as well as for the fabrication of antibody-modified urease nanomotors for efficient penetration of bladder cancer spheroids.[15] Apart from spherical particles, enzymes have been reported to power various other structures, such as supramolecular stomatocytes,[16] polymersomes,[17] carbon nanotubes,[18] silica nanotubes,[19] PEDOT/Au microtubes,[20] polypyrrole/Au nanorods,[21] silk fibroin,[22] and macroscale carbon fibers.[23] Despite significant advances in the field of motors, only a few micro/nanomotors demonstrated motion in oily solution,[24] and enzymatic motors capable of navigating in oil solution or at the oil–water interface are still rarely explored.

Herein, we demonstrate that lipase-powered nanomotors (LNMs), with stochastic binding of lipase on mesoporous silica nanoparticles (MSNPs), can swim in dissolvable triglyceride solution, thus improving the degradation efficiency of slightly dissolvable triglyceride. Lipase (triacylglycerol ester hydrolases from Candida rugosa, EC 3.1.1.3) was chosen for the experiment as lipase can act as a catalyst for the decomposition of triglyceride substrates, both dissolvable (e.g., triacetin with a solubility of 61 mg mL−1) and slightly dissolvable (e.g., tributyrin with a solubility of 0.133 mg mL−1) ones. It offers two functionalities: 1) It acts as the power engine with triacetin as the fuel, and 2) it takes on the role of active cleaner for the tributyrin droplets. In addition to enhancing the motion of LNMs, the triacetin fuel is biocompatible (an FDA-approved food additive[25]) and thus suitable for biological and environmental applications. Furthermore, LNMs present a high efficiency in triglyceride degradation compared with free lipase and other enzymatic motors (see Figure 4).

The LNMs were fabricated using MSNPs as the substrate to immobilize lipase. MSNPs are biocompatible, and their porous structure is useful for drug loading.[26] The surface of the MSNPs was modified chemically using glutaraldehyde as a crosslinker between the amino groups of lipase and MSNPs, respectively (Figure 1 a), resulting in stable catalytic activity.[27] The MSNPs were characterized by transmission electron microscopy (TEM) and scanning electron microscopy (SEM; see the Supporting Information, Figure S1 a, b). They consisted of uniform spheres (Figure 1 b, c) with a porous structure (Figure S1 a, inset) and showed an average diameter of 431.01±1.99 nm (N=100, average diameter±standard error of the mean (SE), see Figure S2). They showed no aggregation, which was also confirmed through dynamic light scattering (DLS). After each modification step, there was only a single population distribution in the hydrodynamic radius plots (Figure S3 a), indicating that the MSNPs were still well dispersed. The increase in hydrodynamic radius and the broader peak can be attributed to the amination and lipase immobilization (Figure S3 a). Furthermore, the change in surface charge confirmed each modification step (Figure 1 d): The as-synthesized MSNPs had a negative surface charge of −16.43±1.36 mV, which increased to 22.57±1.79 mV after amination. Lipase immobilization in PBS solution (phosphate-buffered saline, pH 7.4) caused the surface charge to drop to −7.68±1.21 mV, which can be attributed to the isoelectric point of lipase of about pH 5.6–5.8.[28] Additionally, protein immobilization was characterized by fluorescence staining (Figure 1 e–g). Confocal FL microscopy images show the MSNPs loaded with Rhodamine B (RB) (Figure 1 e) and stained with Krypton (Figure 1 f). Immobilization of lipase on the surface of the MSNPs was also confirmed (Figure 1 g). These results were further corroborated by the presence of a peak at 280 nm in the UV spectrum of the lipase-modified MSNPs (Figure S3 b).[29]

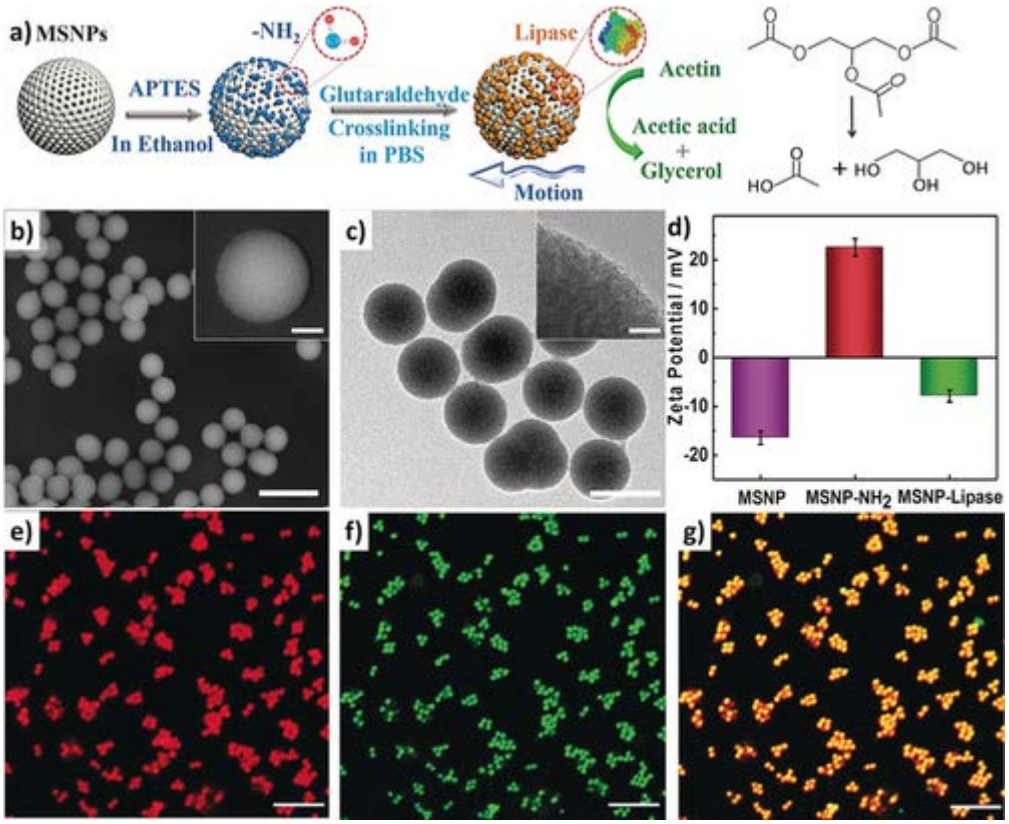

Figure 1

a) Schematic representation of the functionalization strategy for the preparation of the lipase-based nanomotors, whose motion is triggered by the catalytic reaction with triacetin. b) SEM and c) TEM microscopy images of MSNPs modified with lipase, with insets showing magnifications. Scale bars: b) 1 μm (100 nm in the inset), and c) 500 nm (20 nm in the inset). d) Evolution of the surface charge after modifying the MSNP surfaces with amine functional groups, followed by lipase. All measurements were carried out in the same PBS (pH 7.4) solution. e–g) Confocal fluorescence (FL) images of lipase-modified MSNPs, scale bars are 5 μm. The red FL is due to Rhodamine B (RB) loading of the MSNPs, while the green FL is generated by the Krypton-modified lipase. g) The corresponding merged image.

Enzyme assays were carried out to confirm that lipase remained active after its immobilization onto the MSNPs. In the studied motor concentration range of 0.1 to 1.0 mg mL−1, the active milliunits of lipase linearly increased with motor concentration (Figure S4 a), confirming the catalytic activity of the lipase-modified MSNPs. To investigate the motility of the lipase-modified MSNPs in PBS solution, we selected triacetin as the substrate because of its solubility in PBS. As the catalytic reaction of triacetin generates acetic acid [Eq. (1) in the Supporting Information], litmus (10 mg mL−1) was added as a pH indicator to the triacetin (10 mm)-containing PBS solution (pH 7.4, 10 mm) to further confirm the catalytic activity of the LNMs. This was followed by the collection of UV spectra. Initially, that is, prior to the addition of the LNMs, the triacetin PBS solution had a blue color (absorption at 580 nm; Figure S4 b, blue curve), which changed to pink within about 3 h after adding the LNMs (absorption at 500 nm; Figure S4 b, red curve). This further confirmed that lipase maintained its activity after being immobilized on the MSNPs (Figure S5).

We tested different concentrations of triacetin as fuel for the lipase-modified MSNPs. The mean squared displacement (MSD; Figure 2 a), calculated from the tracked trajectories (Figure 2 a, inset), increased linearly with time and fuel concentration, indicating a fuel-concentration-dependent motility.[30] The effective diffusion coefficient (De) was calculated from the MSD per time interval (Δt) as De=0.25 MSD/Δt. During the studied time range, the De value of the lipase-modified MSNPs was 0.72±0.03 μm2 s−1 in PBS solution without adding fuel, increasing to 0.94±0.05, 1.08±0.05, and 1.13±0.04 μm2 s−1 (Figure 2 b) when 1.0, 10, and 100 mm of fuel was added, respectively. This illustrates the increase in De with triacetin concentration. As De increased only marginally (by 4.6 %) when adding 100 mm instead of 10 mm of fuel, we used 10 mm for all subsequent experiments. When adding 10 mm of fuel, the LNMs were capable of a sustained motion for about 40 min (Figure 2 c). After 40 min, the De dropped again to the control value (sample without added fuel; Figure 2 d).

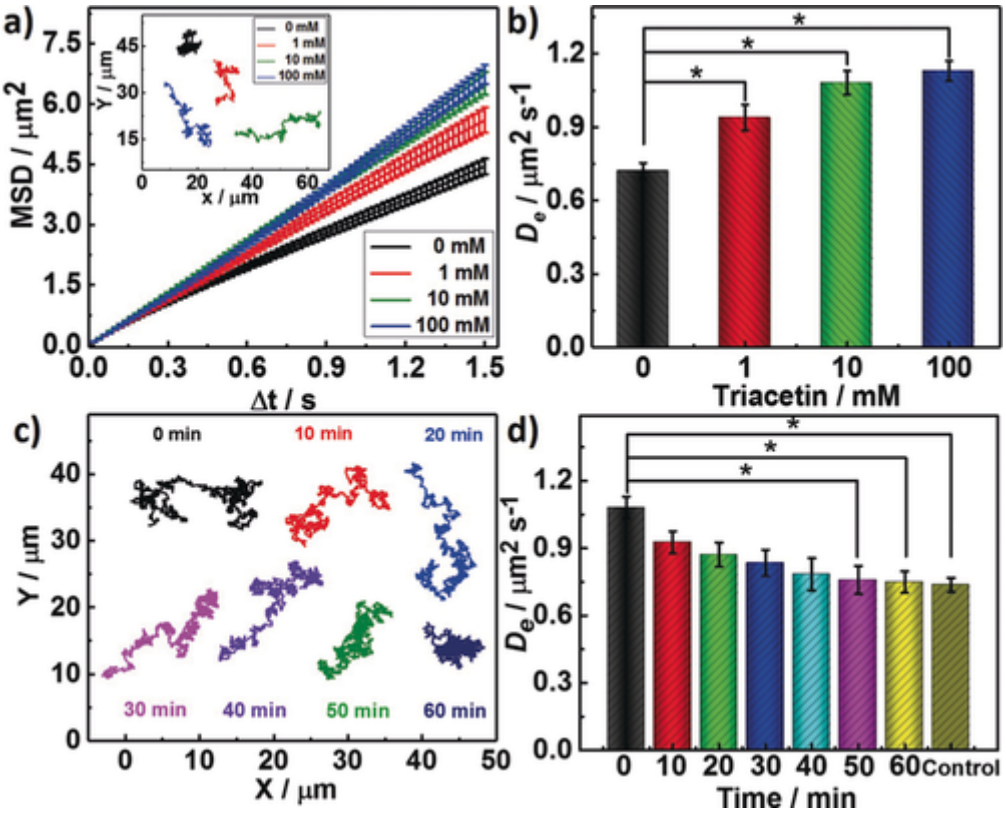

Figure 2

a) Representative trajectories (inset) of LNMs with different triacetin concentrations of 0 mm (black), 1 mm (red), 10 mm (green), and 100 mm (blue) and corresponding mean square displacements (MSDs; n≥20, error bars represent SE). b) Effective diffusion coefficients obtained by analyzing the MSD for different triacetin concentrations. c) Representative trajectories of LNMs at different times with sufficient fuel. d) Diffusion coefficients of LNMs as a function of time, with 100 mm of triacetin. Control experiment: LNMs in PBS solution without fuel. *p<0.05 when compared to the control group.

To explore the ability of LNMs to degrade triglyceride, tributyrin was selected as the removal target as it is slightly dissolvable in PBS solution, thus resembling “blood lipid”. When LNMs (50 μg mL−1) were added to a PBS solution containing tributyrin droplets in suspension (Figure S6), the LNMs exhibited typical Brownian motion with De=0.78±0.043 μm2 s−1 (Figure 3 a–d). This suggests that low tributyrin concentrations (0.133 mg mL−1, saturated concentration) do

not induce enhanced Brownian diffusion of LNMs. After adding fuel (triacetin, 10 mm), the LNMs moved more rapidly, resulting in De=1.096±0.085 μm2 s−1 (Figure 3 b–d). When the LNMs happened to reach the surface of the oil droplets, they were confined at the oil–water interface because of the inherent amphiphility of lipase,[31] but still maintained a diffusion coefficient of De=0.174±0.038 μm2 s−1 (Figure S7), which is significantly smaller than that of Brownian motion in bulk solution. The confinement of LNMs to the oil droplets' surface is shown in Figures 3 e, f and S8, where the interfacial catalysis between lipase and tributyrin occurred. Therefore, the tributyrin droplets were degraded (≤20 μm in diameter) within 1 h.

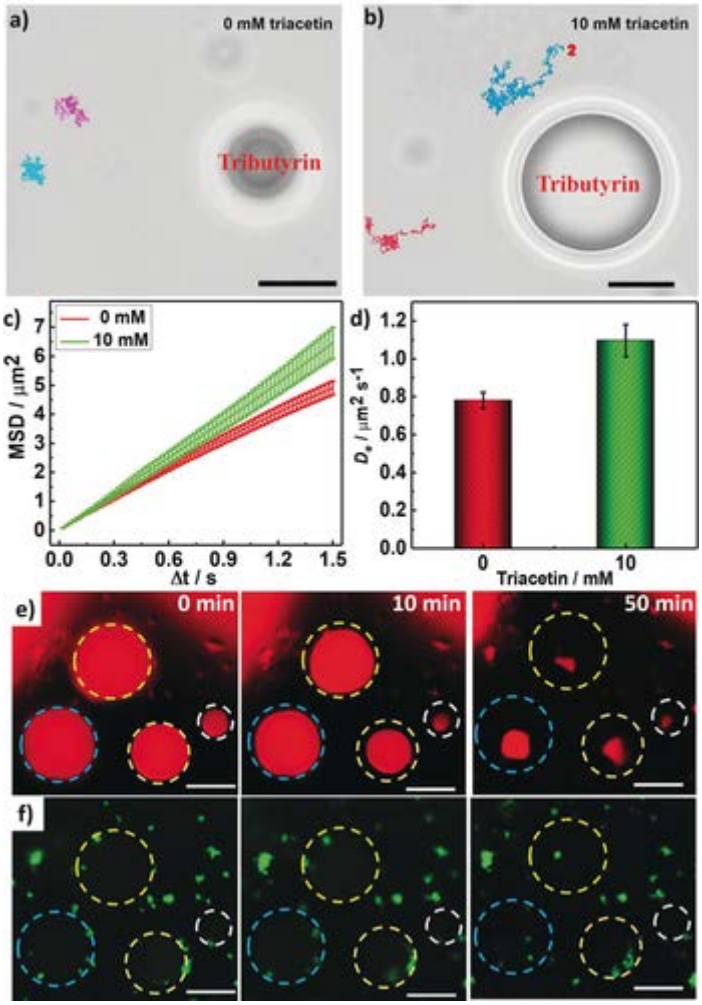

Figure 3

Representative trajectories of lipase motors surrounding tributyrin droplets with a) 0 and b) 10 mm of added triacetin. Scale bars are 5 μm. c) MSDs of the LNMs with 0 and 10 mm triacetin (n≥16, error bars represent the SE). d) Effective diffusion coefficients obtained from the MSD at different triacetin concentrations (with tributyrin droplets present in the solution). e, f) FL microscopy images showing the interaction between the droplets (red FL from Nile Red in tributyrin oil phase) and motors (green FL from FITC loaded in MSNPs) at different times, with dashed circles showing the initial sizes.

To dynamically explore the degradation process, we focused on a single representative tributyrin droplet. Litmus was used to illustrate the dynamic color change during the degradation of tributyrin by LNMs, which produces butyric acid [Figure 4 a, Eq. (2) in the

Supporting Information]. While the fuel-induced catalytic reaction can trigger an immediate local pH change, the color change may be delayed by up to 3 h because of the low fuel concentration (10 mm). However, tributyrin degradation significantly accelerated the acidification, producing a color change in just 30 min. The color of the surrounding solution was simultaneously analyzed by individual channel using Image J software (RGB intensity; see Figure 4 b). Initially, the diameter of a representative tributyrin droplet was about 11.36 μm (Figure 4 d), and the solution exhibited a blueish color (blue intensity (BI): 231.6; red intensity (RI): 160) with a pH value of 7.4 (Figure 4 b, t=0 min). After 10 min, the diameter of the droplet had decreased to 9.65 μm, and the surrounding solution turned purple (Figure 4 a, b, BI: 203.5 and RI: 194.1, pH 4.5). As time progressed, the droplet size continued to decrease, while the surrounding solution turned increasingly red (decreasing BI and increasing RI values). Towards the end of the experiment (50 min), the tributyrin droplet had been degraded, and the solution had changed to pink (BI: 160.0; RI: 207.7) because of the continuous release of butyric acid into the surrounding solution. This represents a visible dynamic demonstration of the tributyrin degradation process (from 0 % to 100 %).

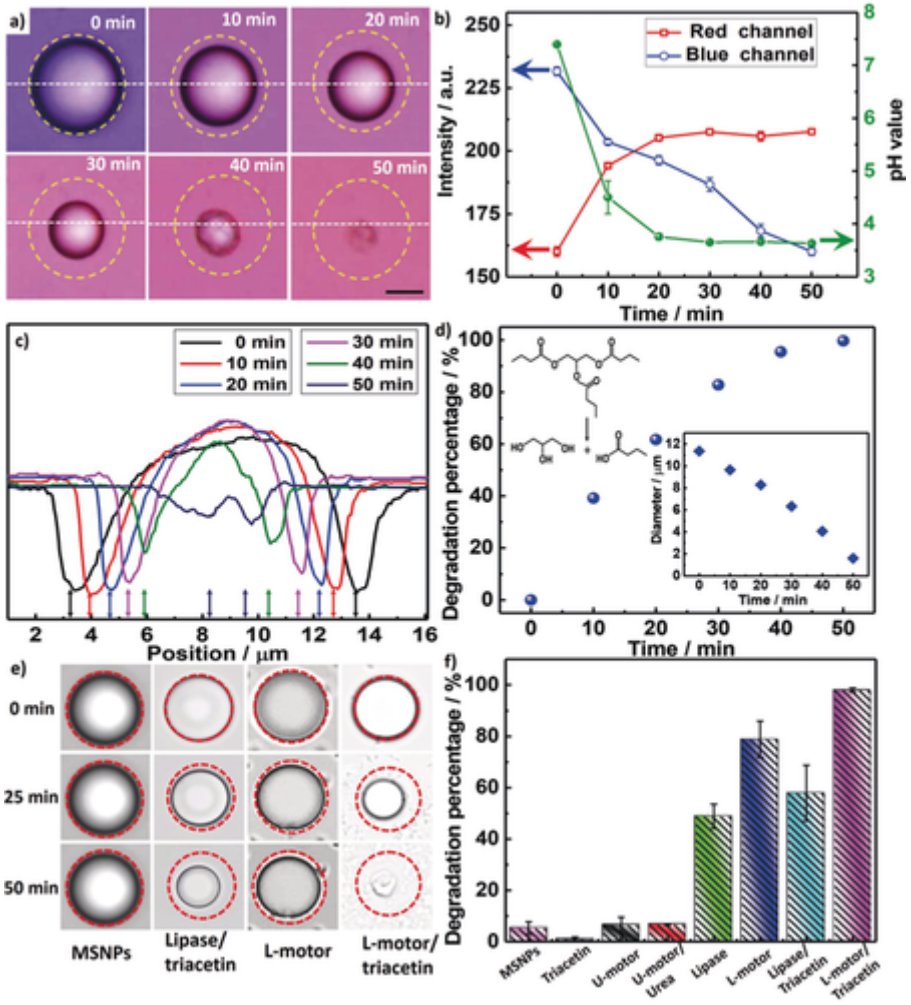

Figure 4

Demonstrating the dynamic degradation process of tributyrin droplets with lipase motors at different times. a) The color change of the surrounding medium is caused by the litmus, indicating the continuous generation of butyric acid. Round dashed circles indicate the initial size of the tributyrin droplets. The scale bar is 5 μm. b) Corresponding RGB intensity and pH value in the surrounding solution. c) Size

measurement of the tributyrin droplets according to the white dashed lines in (a). d) Degradation percentage of tributyrin droplets calculated from their diameters (see inset); the chemical equation shows the catalytic decomposition of tributyrin. e) Optical microscopy of the degradation processes of tributyrin droplets under different conditions. f) Corresponding histogram to (e), showing the degradation percentage of tributyrin droplets under different conditions after 1 h.

To further demonstrate the advantages of LNMs for the degradation of tributyrin, different control experiments were conducted (Figures 4 e, f and S9), including with bare MSNPs, triacetin, urease–MSNP nanomotors, urease–MSNP nanomotors with urea fuel (20 mm), free lipase, free lipase with triacetin, LNMs without fuel, and LNMs with triacetin as fuel (10 mm). Urease nanomotors were chosen as controls because we needed to determine whether enhanced diffusion can improve the degradation. With bare MSNPs, there was only 5.2 % degradation of the droplets after 1 h. This is mainly due to the low tributyrin solubility, indicating that bare MSNPs have almost no effect on tributyrin droplets. Pure triacetin (10 mm), urease–MSNP motors with urea (20 mm), and urease–MSNP motors without urea yielded degradations of 1 %, 6.5 %, and 6.7 %, respectively. We can thus conclude that urease–MSNP nanomotors, despite containing enzymes on the surface and presenting enhanced diffusion, cannot degrade tributyrin droplets. Additionally, we also compared the affinities of urease motors and LNMs for targeting the tributyrin droplets. The same concentration of MSNPs was later separated into two aliquots, which were loaded with fluorescein isothiocyanate (FITC), followed by the corresponding modification with urease and lipase, respectively. After these two types of FITC-loaded nanomotors had been added into the solution containing tributyrin droplets, we calculated the FL intensity on the tributyrin droplet area (see the Supporting Information and Figures S10 and S11 for details). Initially, both types of motors were distributed randomly in the solution (Figure S10) with a similar FL intensity within the droplet area. Within 1 h, the FL intensity surrounding the droplet area increased dramatically in the presence of fuel for the LNMs (Figure S11), confirming that LNMs tend to accumulate on the surface of tributyrin droplets, which leads to their highly efficient degradation. Besides, with free lipase (2 μg mL−1), the droplet degradation was 48.9 %, which increased to 57.9 % after adding triacetin, thus illustrating the enhanced degradation process in the presence of fuel due to the enhanced diffusion of free lipase. LNMs (50 μg mL−1) with 2 μg mL−1 lipase (measured through bicinchoninic acid assay (BCA), details in the Supporting Information) can lead to a 78.8 % degradation, which is higher than that with free lipase. This is due to the fact that free lipase tends to form bimolecular aggregates that partially block the lipase active centers, which in turn results in a less active form.[32] The immobilization can be beneficial for cleaving these lipase dimers, thus improving their efficiency. Notably, more than 98 % of the droplets can be degraded through the addition of triacetin, which demonstrates how lipase anchored to MSNPs increases the efficient propulsion and diffusion towards the target.

In conclusion, we have demonstrated that the lipase-based catalytic reaction can be utilized to provide MSNPs with enhanced motility in triglyceride-containing PBS solutions. Compared to free lipase and urease nanomotors, we showed that active lipase nanomotors can accelerate the degradation of tributyrin droplets to a very high degree (ca. 98 % within 50 min). These results hint towards possible new applications of lipase-powered nanomotors, in biomedicine for high-triglyceride-related diseases or in environmental remediation for oil removal. However, it is necessary to understand the stability and activity of such motors in oil-polluted waters, as well as the interaction of these motors with adipocytes. Future work should be dedicated to improving the motion control, as well as their performance in biological fluids, such as serum or blood.

Acknowledgements

We thank Albert Miguel López and Lucas Santiago Palacios Ruiz for the development of the tracking and extracting software, respectively. L.W. thanks the NSFC (No. 51703043), the Marie Skłodowska-Curie fellowship (Grant No. 712754), and the Severo Ochoa programme (Grant SEV-2014-0425 (2015–2019)). A.C.H. thanks MINECO for a Severo Ochoa fellowship. X.H. thanks the NSFC (No. 21871069). S.S. thanks the Spanish MINECO for grants CTQ2015-68879-R (MICRODIA) and CTQ2015-72471-EXP (Enzwim).

Conflict of interest

The authors declare no conflict of interest.

References

1a. J. Wang, Nanomachines: fundamentals and applications, Wiley, Hoboken, 2013;

1b. S. Balasubramanian, D. Kagan, C.-M. Jack Hu, S. Campuzano, M. J. Lobo-Castañon, N. Lim, D. Y. Kang, M. Zimmerman, L. Zhang, J. Wang, Angew. Chem. Int. Ed. 2011, 50, 4161– 4164; Angew. Chem. 2011, 123, 4247– 4250.

2a. M. Moreno-Guzman, A. Jodra, M.-Á. López, A. Escarpa, Anal. Chem. 2015, 87, 12380– 12386;

2b. X. Yang, Y. Tang, S. D. Mason, J. Chen, F. Li, ACS Nano 2016, 10, 2324– 2330.

3a. J. Shao, M. Xuan, H. Zhang, X. Lin, Z. Wu, Q. He, Angew. Chem. Int. Ed. 2017, 56, 12935– 12939; Angew. Chem. 2017, 129, 13115– 13119;

3b. M. Medina-Sánchez, H. Xu, O. G. Schmidt, Ther. Delivery 2018, 9, 303– 316.

4a. J. Orozco, D. Vilela, G. Ramírez, Y. Fedorak, A. Escarpa, R. Duhalt, J. Wang, Chem. Eur. J. 2014, 20, 2866– 2871;

4b. J. Parmar, D. Vilela, K. Villa, J. Wang, S. Sánchez, J. Am. Chem. Soc. 2018, 140, 9317– 9331.

5a. W. Qin, T. Peng, Y. Gao, F. Wang, X. Hu, K. Wang, J. Shi, D. Li, J. Ren, C. Fan, Angew. Chem. Int. Ed. 2017, 56, 515– 518; Angew. Chem. 2017, 129, 530– 533;

5b. L. Wang, Y. Liu, J. He, M. J. Hourwitz, Y. Yang, J. T. Fourkas, X. Han, Z. Nie, Small 2015, 11, 3762– 3767;

5c. Y. Wu, T. Si, C. Gao, M. Yang, Q. He, J. Am. Chem. Soc. 2018, 140, 11902– 11905.

6. J. Guo, J. J. Gallegos, A. R. Tom, D. Fan, ACS Nano 2018, 12, 1179– 1187.

7a. T. Xu, F. Soto, W. Gao, V. Garcia-Gradilla, J. Li, X. Zhang, J. Wang, J. Am. Chem. Soc. 2014, 136, 8552– 8555;

7b. D. Zhou, Y. Gao, J. Yang, Y. C. Li, G. Shao, G. Zhang, T. Li, L. Li, Adv. Sci. 2018, 1800122.

8a. M. Pal, N. Somalwar, A. Singh, R. Bhat, S. M. Eswarappa, D. K. Saini, A. Ghosh, Adv. Mater. 2018, 30, 1800429;

8b. T. Xu, J. Yu, X. Yan, H. Choi, L. Zhang, Micromachines 2015, 6, 1346– 1364.

9a. C. Chen, F. Mou, L. Xu, S. Wang, J. Guan, Z. Feng, Q. Wang, L. Kong, W. Li, J. Wang, Q. Zhang, Adv. Mater. 2017, 29, 1603374;

9b. M. Xuan, R. Mestre, C. Gao, C. Zhou, Q. He, S. Sánchez, Angew. Chem. Int. Ed. 2018, 57, 6838– 6842; Angew. Chem. 2018, 130, 6954– 6958;

9c. R. Dong, Q. Zhang, W. Gao, A. Pei, B. Ren, ACS Nano 2015, 10, 839– 844;

9d. J. Wang, Z. Xiong, J. Zheng, X. Zhan, J. Tang, Acc. Chem. Res. 2018, 51, 1957– 1965.

10a. T. Patiño, X. Arqué, R. Mestre, L. Palacios, S. Sánchez, Acc. Chem. Res. 2018, 51, 2662– 2671;

10b. X. Zhao, K. Gentile, F. Mohajerani, A. Sen, Acc. Chem. Res. 2018, 51, 2373– 2381;

10c. X. Ma, A. C. Hortelão, T. Patiño, S. Sánchez, ACS Nano 2016, 10, 9111– 9122.

11a. H. S. Muddana, S. Sengupta, T. E. Mallouk, A. Sen, P. J. Butler, J. Am. Chem. Soc. 2010, 132, 2110– 2111;

11b. S. Sengupta, K. K. Dey, H. S. Muddana, T. Tabouillot, M. E. Ibele, P. J. Butler, A. Sen, J. Am. Chem. Soc. 2013, 135, 1406– 1414.

12. K. K. Dey, X. Zhao, B. M. Tansi, W. J. Méndez-Ortiz, U. M. Córdova-Figueroa, R. Golestanian, A. Sen, Nano Lett. 2015, 15, 8311– 8315.

13a. X. Ma, A. Jannasch, U.-R. Albrecht, K. Hahn, A. Miguel-López, E. Schäffer, S. Sánchez, Nano Lett. 2015, 15, 7043– 7050;

13b. X. Ma, X. Wang, K. Hahn, S. Sánchez, ACS Nano 2016, 10, 3597– 3605;

13c. X. Ma, S. Sánchez, Tetrahedron 2017, 73, 4883– 4886.

14a. T. Patiño, N. Gracia, X. Arqué, A. Miguel-López, A. Jannasch, T. Stumpp, E. Schäffer, L. Albertazzi, S. Sánchez, J. Am. Chem. Soc. 2018, 140, 7896– 7903;

14b. T. Patino, A. Porchetta, A. Jannasch, A. Lladó, T. Stumpp, E. Schäffer, F. Ricci, S. Sánchez, Nano Lett. 2019, https://doi-org.sire.ub.edu/10.1021/acs.nanolett.8b04794.

15a. A. C. Hortelão, T. Patiño, A. Perez-Jiménez, À. Blanco, S. Sánchez, Adv. Funct. Mater. 2018, 28, 1705086;

15b. A. C. Hortelão, R. Carrascosa, N. Murillo-Cremaes, T. Patiño, S. Sánchez, ACS Nano 2019, 13, 429– 439.

16. L. Abdelmohsen, M. Nijemeisland, G. Pawar, G. Janssen, R. J. Nolte, J. van Hest, D. Wilson, ACS Nano 2016, 10, 2652– 2660.

17. A. Joseph, C. Contini, D. Cecchin, S. Nyberg, L. Ruiz-Perez, J. Gaitzsch, G. Fullstone, X. Tian, J. Azizi, J. Preston, G. Volpe, G. Battaglia, Sci. Adv. 2017, 3, e 1700362.

18. D. Pantarotto, W. R. Browne, B. L. Feringa, Chem. Commun. 2008, 1533– 1535.

19. X. Ma, A. C. Hortelao, A. Miguel-López, S. Sánchez, J. Am. Chem. Soc. 2016, 138, 13782– 13785.

20. J. Orozco, V. García-Gradilla, M. D'Agostino, W. Gao, A. Cortés, J. Wang, ACS Nano 2013, 7, 818– 824.

21. I.-A. Pavel, A.-I. Bunea, S. David, S. Gáspár, ChemCatChem 2014, 6, 866– 872.

22. D. A. Gregory, Y. Zhang, P. J. Smith, X. Zhao, S. J. Ebbens, Small 2016, 12, 4048– 4055.

23. N. Mano, A. Heller, J. Am. Chem. Soc. 2005, 127, 11574– 11575.

24a. M. Guix, J. Orozco, M. García, W. Gao, S. Sattayasamitsathit, A. Merkoçi, A. Escarpa, J. Wang, ACS Nano 2012, 6, 4445– 4451;

24b. C. Liang, C. Zhan, F. Zeng, D. Xu, Y. Wang, W. Zhao, J. Zhang, J. Guo, H. Feng, X. Ma, ACS Appl. Mater. Interfaces 2018, 10, 35099– 35107.

25. “Final report on the safety assessment of triacetin”: M. Z. Fiume, Cosmetic Ingredients Review Expert Panel, Int. J. Toxicol. 2003, 22, 1– 10.

26. Y. Wang, Q. Zhao, N. Han, L. Bai, J. Li, J. Liu, E. Che, L. Hu, Q. Zhang, T. Jiang, Nanomedicine 2015, 11, 313– 327.

27. W. Xie, X. Zang, Food Chem. 2016, 194, 1283– 1292.

28. K. Veeraragavan, B. F. Gibbs, Biotechnol. Lett. 1989, 11, 345– 348.

29. H. Edelhoch, Biochemistry 1967, 6, 1948– 1954.

30. G. Dunderdale, S. Ebbens, P. Fairclough, J. Howse, Langmuir 2012, 28, 10997– 11006.

31. L. Wang, Y. Lin, Y. Zhou, H. Xie, J. Song, M. Li, Y. Huang, X. Huang, S. Mann, Angew. Chem. Int. Ed. 2019, 58, 1067; Angew. Chem. 2019, 131, 1079.

32. R. C. Rodrigues, C. Ortiz, Á. Berenguer-Murcia, R. Torres, R. Fernández-Lafuente, Chem. Soc. Rev. 2013, 42, 6290– 6307.

Supporting information

Contents

Experimental details 1
1. Materials 1
2. Equipment 2
3. Synthesis of fully Mesoporous Silica Nanoparticles (MSNPs) 2
4. Amine Functionalization of MSNPs (MSNP-NH_2) 3
5. Functionalization of MSNP-NH_2 with Lipase or Urease 3
6. Hydrodynamic Radii and Zeta potential measurement 3
7. Quantification of Lipase Amount on MSNPs 4
8. Activity Assay of L-MSNPs 4
9. Optical Video Recording of Nanomotors and MSD Analysis 4
10. Preparation of the tributyrin droplets 5
11. Calculation of degradability of oil droplets 5
12. Color intensity collection from the obtained images 5
13. FL intensity calculation from the obtained images 5
14. Catalytic reaction equations for triacetin and tributyrin 6
Supporting figures 7
Captions for supporting videos: 14

Experimental details

1. Materials

Methanol (MeOH, 99%), hydrochloric acid (HCl, 37% in water), Ethanol (EtOH, 99%), ammonium hydroxide (25% in water), tetraethylorthosilicate (TEOS, 99%), triethanolamine (TEOA, 99%), cetyltrimethylammonium bromide (CTAB, 99%), 3-aminopropyltriethoxysilane (APTES, 99%), glutaraldehyde (GA, 25% in water), urease (from Canavalia ensiformis, Type IX, powder, 50 000-100 000 units/g solid), lipase (from *Candida Rugose*, Type VII, ≥700 unit/mg solid), Lipase Activity Assay Kit (Sigma-Aldrich), urea (99.9%), triacetin (99%), tributyrin (97%), Rhodamine B (1 mg/mL) were all purchased from Sigma-Aldrich. BCA Protein Assay Kit, phosphate buffer saline (PBS) and Krypton Fluorescent Protein Stain were purchased from ThermoFisher Scientific Company.

2. Equipment

Transmission Electron Microscopy (TEM) images were taken using a JEOL JEM-2100 microscope from University of Barcelona. Scanning Electron Microscopy (SEM) images were obtained by a FEI NOVA NanoSEM 230, from the core facilities of IBEC. Hydrodynamic radii and Zeta potential measurements were performed using a Nano-ZS of Zetasizer system (Malvern Panalytical). Optical videos and droplets images were taken using an inverted optical microscope (Leica DMi8). Protein quantification and enzymatic activity assays were carried out using an Infinite M200 PRO Multimode Microplate Reader. The confocal microscopy analysis was performed using an LSM 800-Zeiss equipped with a 63× oil objective, from the core facilities of IBEC.

3. Synthesis of fully Mesoporous Silica Nanoparticles (MSNPs)

The sol-gel method was utilized for the preparation of MSNPs, with cetyltrimethylammonium bromide (CTAB) as the porogenic agent and triethanolamine (TEOA) as the base catalyst. In brief, a solution containing CTAB (570 mg), TEOA (35 g), and water (20 mL) was heated to 95 °C in a silicon oil bath under continuous stirring for 30 min, followed by the dropwisely addition of TEOS (1.5 mL). Later on, the mixed solution was kept stirred for 2 h at 95 °C, followed by the collection via centrifugation and washing for 3 times using EtOH (1350 *g*, 10 min), with 10 min sonication between each washing. Then the obtained particles were resuspended in a solution of MeOH:HCl (10:0.6 v/v, 30 mL) and refluxed for 24 h at 80 °C, in order to remove the additional CTAB from the MSNPs' cores. Subsequently, the particles are collected by centrifugation and washed in ethanol (3 times, 1350 *g*, 10 min), with sonication for 10 min between each centrifugation. Finally, aliquots (0.5 mL) were collected, centrifuged and air-dried to determine the concentration of the MSNPs suspension.

4. Amine Functionalization of MSNPs (MSNP-NH_2)

The previously synthesized MSNPs were suspended in EtOH (2 mg/mL), and sonicated for 10 min, followed by the addition of APTES (10 µL/mg of MSNP) directly into the solution. The mixture was strongly stirred for 24 h at room temperature with an end-to-end rotary shaker. Then, the functionalized particles were centrifuged and washed in ethanol for 3 times (1350 g, 10 min) and in water for 3 times (1928 g, 10 min), respectively, with sonication for 20 min between each centrifugation. Finally, aliquots (0.5 mL) were collected, centrifuged and air-dried to determine the concentration of the MSNPs suspension.

5. Functionalization of MSNP-NH_2 with Lipase or Urease

MSNP-NH_2 were centrifuged at 1340 g for 10 min, resuspended in 900 µL of PBS (5 mg/mL) and sonicated for 20 minutes, followed by the addition of 100 µL glutaraldehyde and vortexed for 30s. Then the mixture was strongly shaken using a vortex shaker for 3h at room temperature. The solution will give a pink color after 3h, and then the solution was washed using PBS (1340 g, 10 min) for 3 times with sonication for 20 min between each washing. Subsequently, the GA-activated nanoparticles were suspended in PBS solution containing lipase (8 mg/mL) or urease (3 mg/mL), respectively. The mixture was put on a vortex shaker overnight at room temperature at a speed of 1500 r/min. Finally, the obtained nanomotors was washed 3 times using PBS by centrifugation (1340 g, 10 minutes), intercalating the washes with 1 min of vortex and 3 min of sonication.

6. Hydrodynamic Radii and Zeta potential measurement

The tests of the size distribution and zeta potential of MSNP, MSNP-NH_2, and MSNP-lipase were conducted using a Morphologi 4-ID (Malvern Panalytical) system. The samples were diluted to a concentration 0.5 mg/mL and then analyzed for light scattering and zeta potential, with an acquisition time of 5 s, performing 3 runs per measurement. A total of 9 measurements were performed to obtain statistical relevant data.

7. Quantification of Lipase Amount on MSNPs

The BCA Protein Assay Kit from ThermoFisher Scientific was utilized for the quantitation of lipase amount on the MSNPs, following the manufacturer's instructions. BCA quantifies the total protein amount by quantifying the reduction of Cu^{2+} to Cu^{1+} by protein's peptide bonds. After reaction, the BCA solution forms a purple-blue complex with Cu^{1+} in alkaline environments, thus providing a quantification process.

8. Activity Assay of L-MSNPs

The lipase activity after immobilized on MSNPs was determined using the lipase activity assay kit (Catalog Number MAK046) from Sigma-Aldrich, following the technical bulletin. The quantification was realized based on the lipase catalytic reaction, *i.e.*, the cleavage of the ester bonds of lipids. Briefly, the lipase activity is determined using a coupled enzyme reaction, which results in a colorimetric (570 nm) product proportional to the enzymatic activity present. Accordingly, one unit of lipase is the amount of enzyme which could generate 1.0 µmol of glycerol from triglycerides per minute at 37 °C. All the calculations were carried out according to the technical bulletin.

9. Optical Video Recording of Nanomotors and MSD Analysis

An inverted microscope equipped with a 63× water objective was used to observe and record videos of the motion of nanomotors. The lipase-MSNPs nanomotors with different concentrations of triacetin were put on a glass slide and mixed well, followed by covering with another glass slide. Then each sample was videoed for 30 s by a Hamamatsu camera with a frame rate of 50 fps.

A self-edited python-based code was developed to obtain the trajectories of the nanomotors from the obtained videos, and the mean-squared displacement (MSD) and the diffusion coefficient (D_e) was calculated using the following equations:

$$MSD\ (\Delta t) = \langle (x\_i\ (t+\Delta t)-x\_i\ (t))\text{^}2 \rangle$$

$$MSD\ (\Delta t) = 4\ D_e\ \Delta t,$$

where, i = 2, for 2D analysis; D_e represents the effective diffusion coefficient and Δt represents the time interval.

10. Preparation of the tributyrin droplets

The tributyrin droplets were easily obtained by strongly hand-shaking the tributyrin/PBS mixture (50:2, v/v) for 1 min, shown in Figure S5. Typically, 500 µL PBS solution and 20 µL tributyrin were added into a 1.5 mL Eppendorf tube, followed by strongly hand-shaking for 1 min. Then the solution was used for the mimicry of lipid storage droplet.

11. Calculation of degradability of oil droplets

The images taken using Leica microscope were analyzed using Image J, for measuring the diameter of the droplet before (D_B) and after (D_A) the catalytic reaction cause by different conditions. The degradability was calculated using the following equation:

$$\text{Degradability percentage} = [(D_B\text{^}3 - D_A\text{^}3) / D_B\text{^}3] * 100\%$$

12. Color intensity collection from the obtained images

The RGB intensity of the colorful images were collected using Image J software (Version 6.0.0.260) by drawing lines across the images, followed by the calculation of the average intensity.

13. FL intensity calculation from the obtained images

To determine the FL intensity on the droplets, due to the attachment of FITC loaded Lipase-nanomotors or Urease-nanomotors, Image J software (Version 6.0.0.260) was utilized, using the following equation:

Corrected total FL= Integrated Density-(Area of selected droplets× Mean FL of background readings)

Where, corrected total FL is the calculated FL results, the integrated density was the value of the pixels in the image or selection area, and background readings are the values of the pixels of a background in the image or selection area.

14. Catalytic reaction equations for triacetin and tributyrin

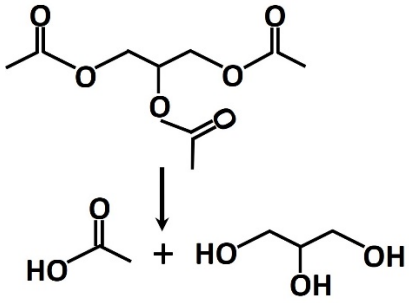

(Equation 1, triacetin)

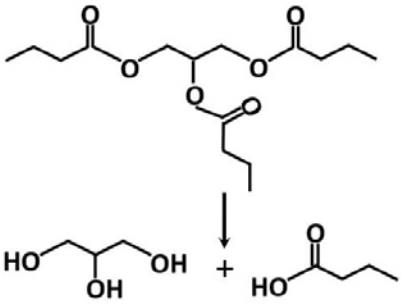

(Equation 2, tributyrin)

Supporting figures

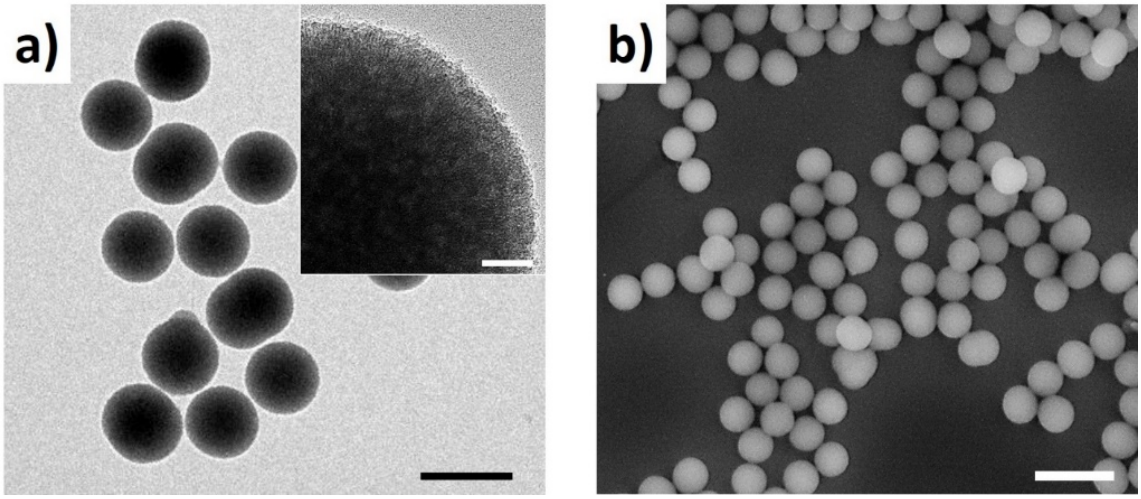

Fig. S1 TEM (a) and SEM (b) images of MSNPs. Scale bars are 500 nm and 1 um in a) and b), and 30 nm in the inset, respectively.

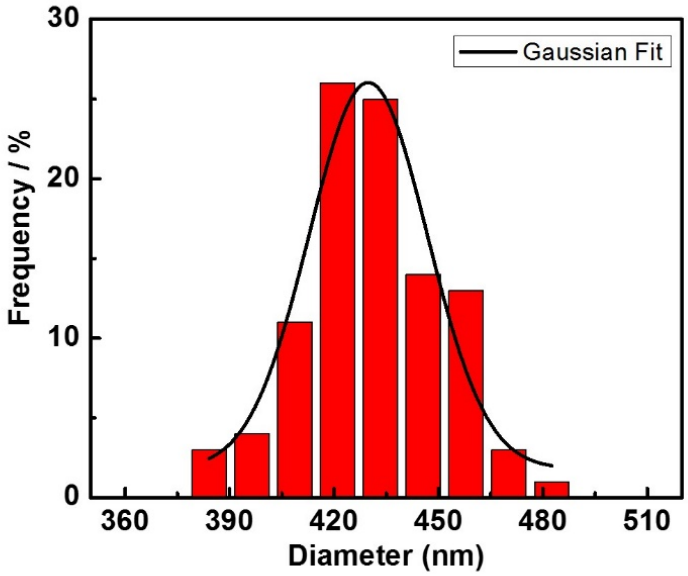

Fig. S2 The histogram of MSNPs size distribution evaluated by SEM image, with the Gaussian fit curve.

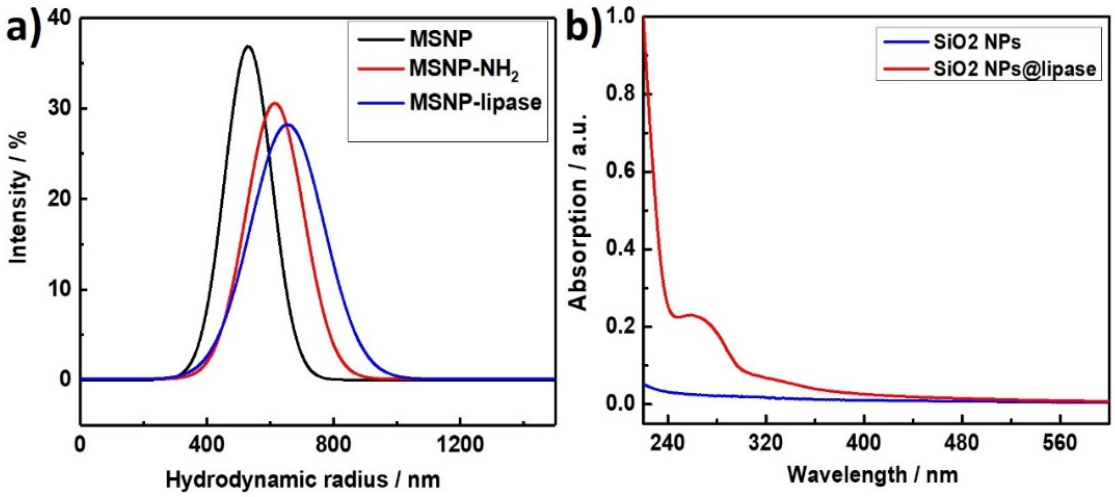

Fig. S3 (a) Hydrodynamic radii plots of the surface modification of the MSNPs with amine functional groups, followed with lipase. (b) UV absorption plots of bare MSNPs and MSNPs-lipase.

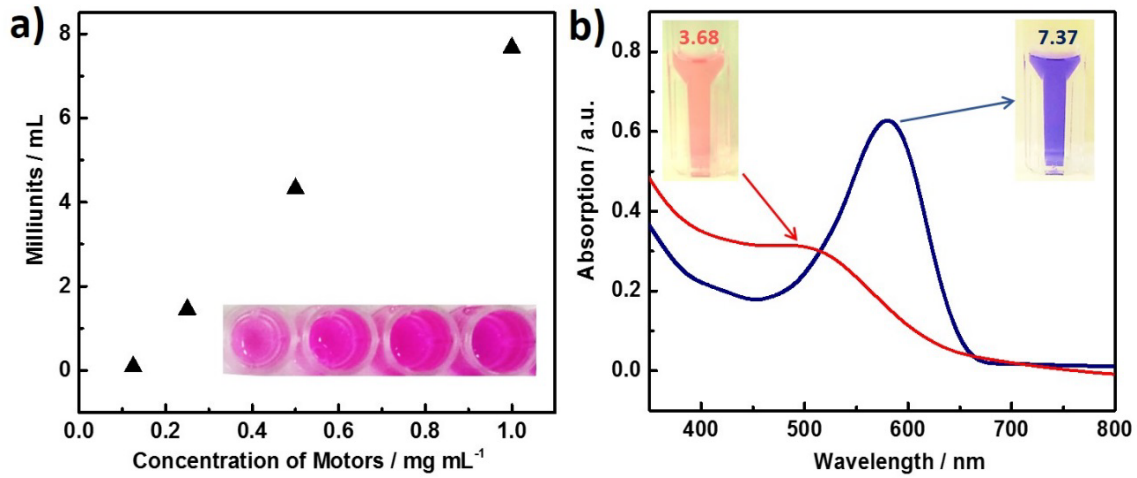

Fig. S4 Analysis of the activity of lipase after modification and the motion behavior of lipase-powered nanomotors. (a) The milliunits of lipase as a function of the concentration of L-MSNPs, obtained using lipase assay kit from Sigma (inset). (b) The UV absorption curves of the triacetin solution (100 mM/mL) with litmus (10 mg/mL) before and after the addition of L-MNSPs, with the photos showing the solution colors and corresponding pH values.

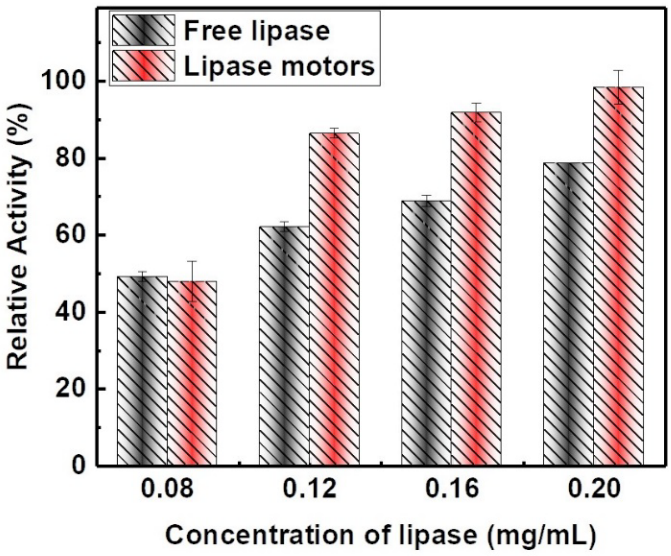

Fig. S5 Comparison between the relative activity of free lipase and bound to MSNP in PBS solution after 50 minutes reaction.

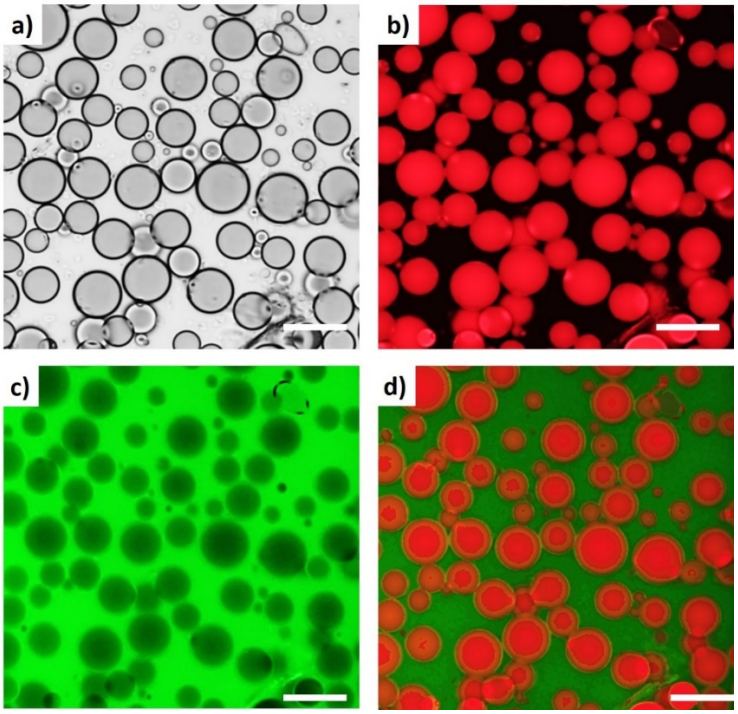

Fig. S6 The optical (a), fluorescence (b, c) and corresponding merged images of the tributyrin droplets in PBS solution (pH 7.4), obtained by hand-shaking. Scale bars are 20 μm. The green fluorescence is generated from FITC in water, and the red fluorescence is from Nile Red in the oil phase.

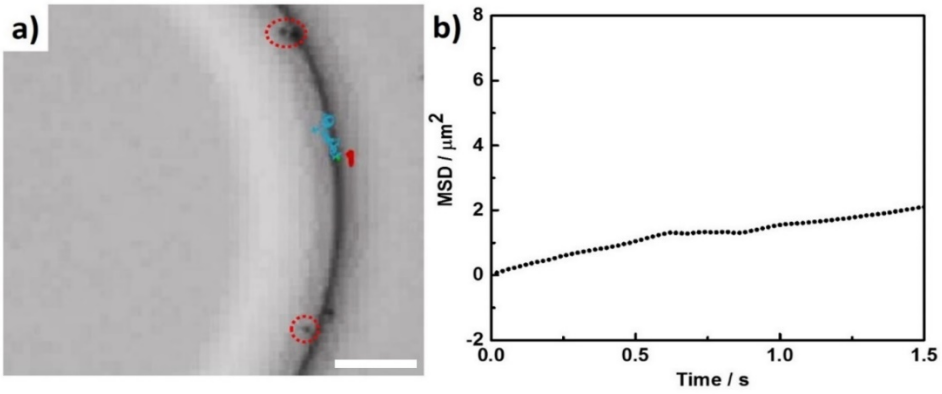

Fig. S7 The optical image of the tributyrin droplet with motors attached on the surface. The representative trajectory shows the motor moves on the surface, with the corresponding MSD shown in (b). The diffusion coefficient calculated was 0.174±0.038 $\mu m^2/s$, which was much smaller than that of Brownian motion, indicating the motor was confined on the surface of the droplet, but moving slower probably due to the viscosity of the droplet. The red dash circles show other motors confined on the surface of the droplets. The scale bar is 3 μm.

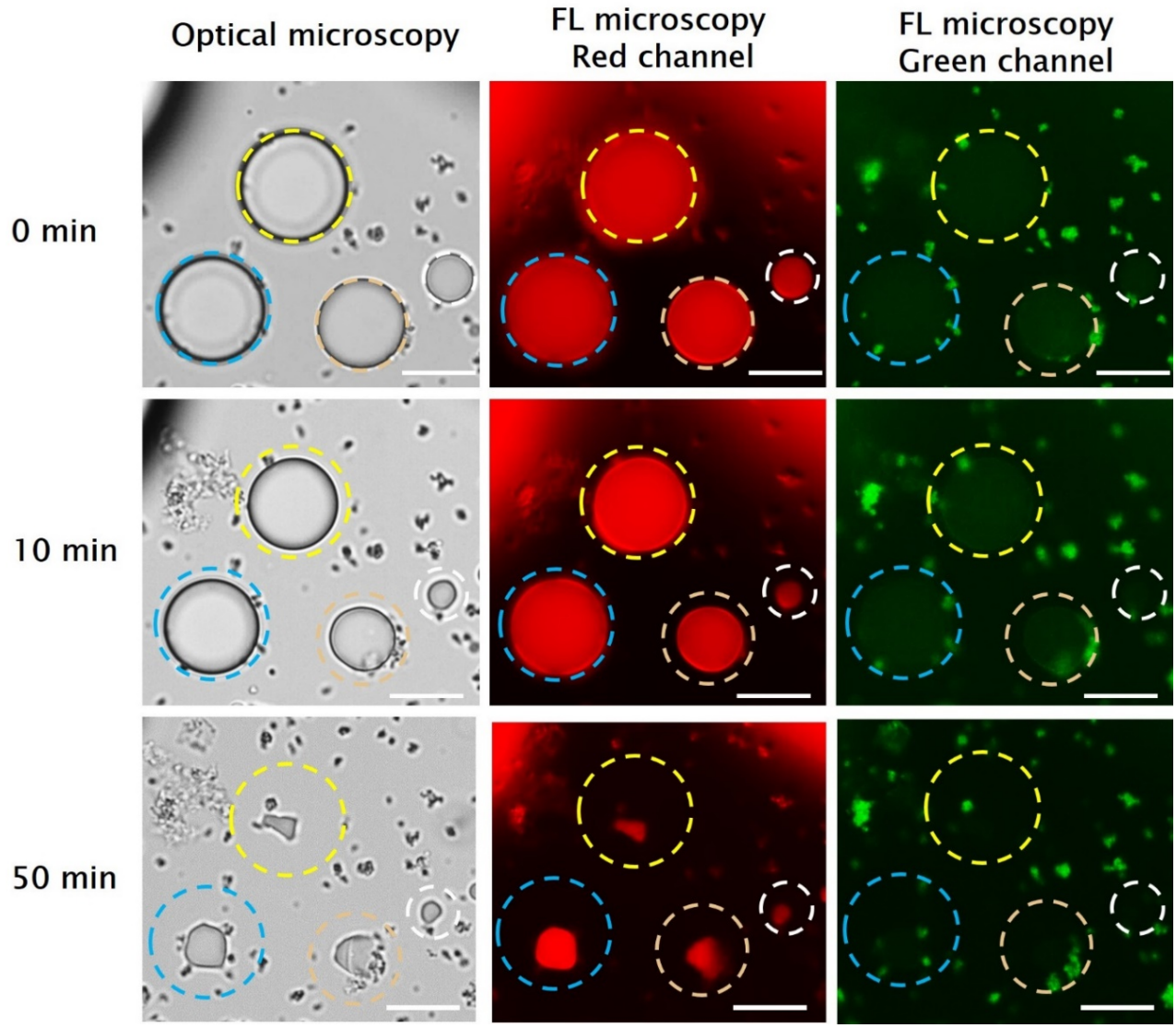

Fig. S8 The optical (a) and fluorescence (b, c) images of the tributyrin droplets in PBS solution (pH 7.4) during the degradation process using lipase motors. The red FL is generated by Nile red in the oil phase, while the green FL is due to the loading of FITC into the MSNPs. Dash circles with different colors showed the initial corresponding size of each different droplet. Scale bars are 5 μm.

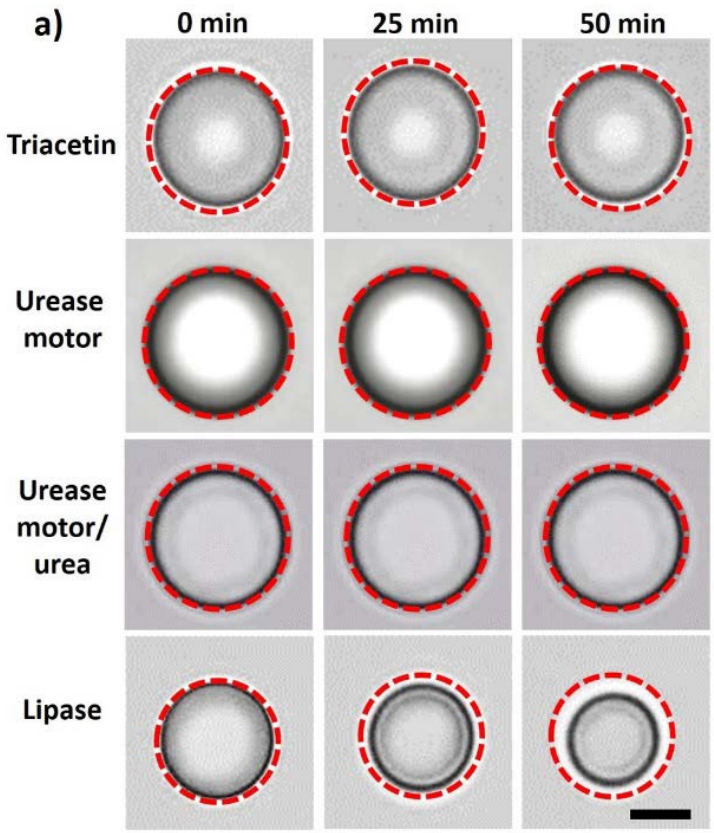

Fig. S9 (a) Optical microscopy images showing the degradation processes of tributyrin droplets under control conditions, including pure triacetin, urease motor, urease motor with urea (20 mM), and pure lipase (2 μg/mL). The dash circles show the initial size of the droplets at different conditions.

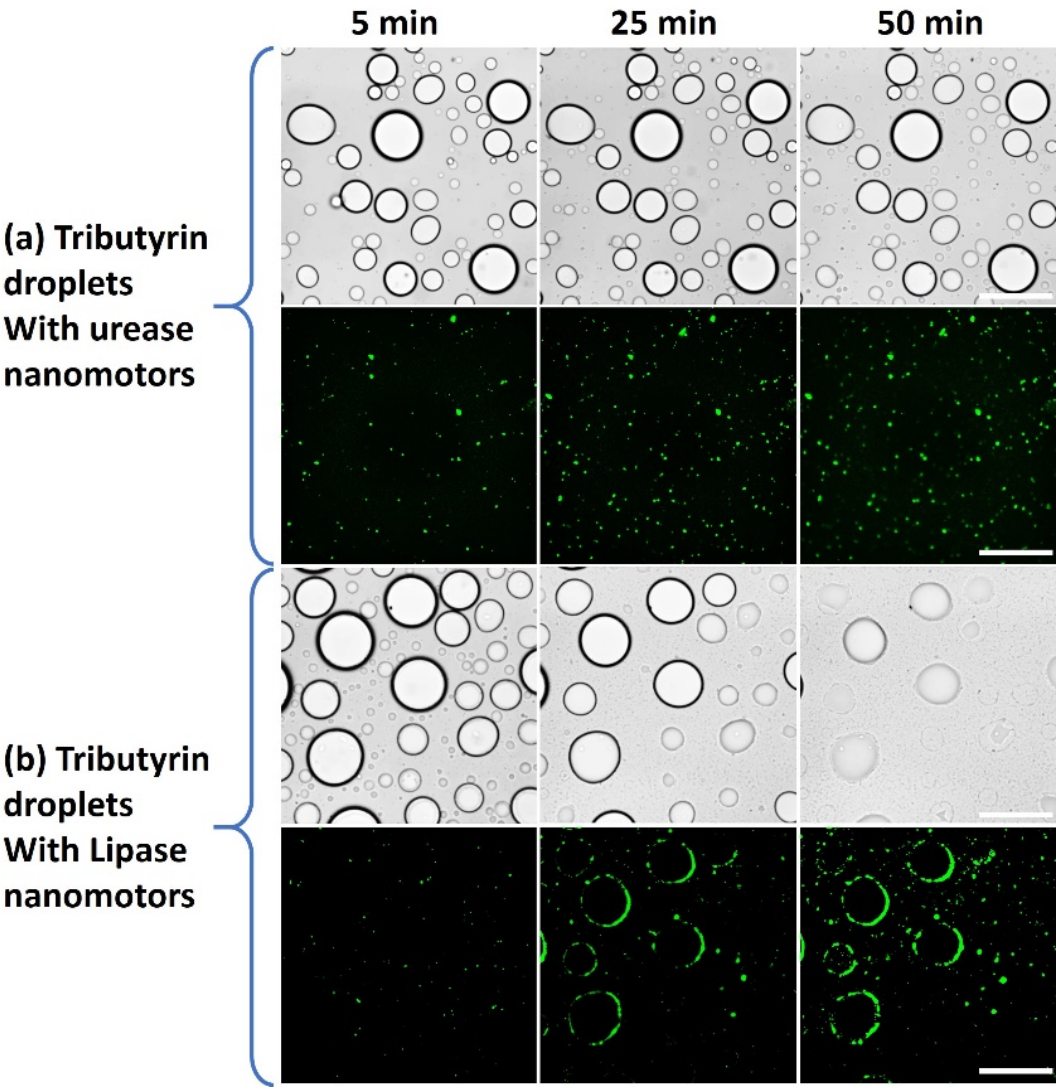

Fig. S10 The optical and fluorescence images of the tributyrin droplets in PBS solution (pH 7.4) with the same concentration of (a) urease nanomotors/urea (20 mM) and (b) lipase nanomotors/triacetin (10 mM) within 55 min, showing the lipase motors tend to sediment surrounding the tributyrin droplets. Scale bars are 20 μm.

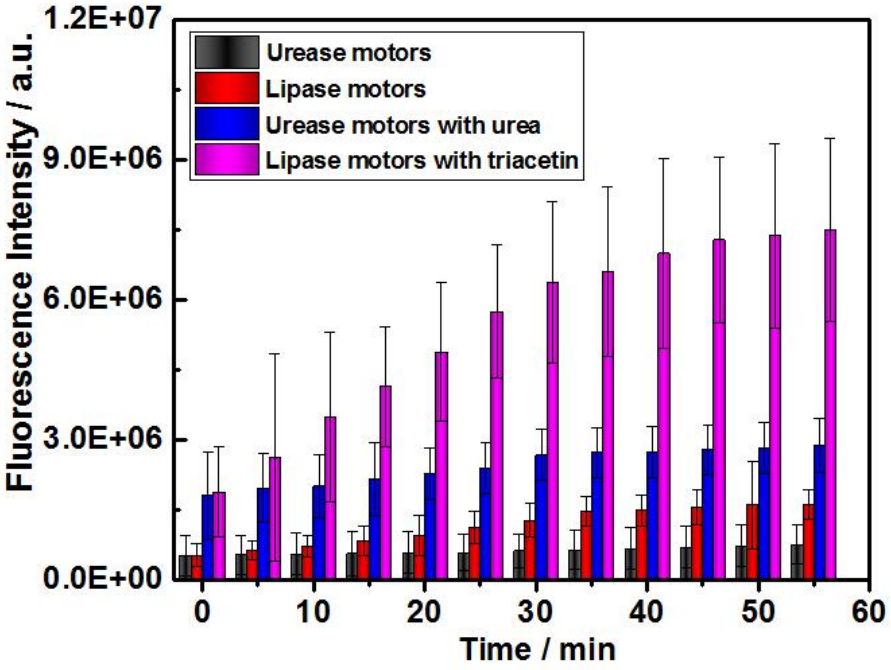

Fig. S11 The profile of calculated fluorescence intensity of the Urease and Lipase nanomotors with and without corresponding fuel on the surface of tributyrin droplets in PBS solution (pH 7.4), within 55 min.

Captions for supporting videos:

Video S1, Representative lipase motor with tracked trajectory in PBS solution without fuel;

Video S2, Representative lipase motor with tracked trajectory in PBS solution with 1 mM triacetin;

Video S3, Representative lipase motor with tracked trajectory in PBS solution with 10 mM triacetin;

Video S4, Representative lipase motor with tracked trajectory in PBS solution with 100 mM triacetin;

Video S5, Tributyrin droplets degradation (16X acceleration) using lipase motors (50 μg/mL), with the colour change of surrounding solution.